Biomedical Optics EXPRESS

Development and optimization of near-IR contrast agents for immune cell tracking

Pratixa P. Joshi,[1] Soon Joon Yoon,[1] Yun-Sheng Chen,[1] Stanislav Emelianov,[1,2] and Konstantin V. Sokolov[1,2,*]

[1] *Department of Biomedical Engineering, University of Texas at Austin, 107 W Dean Keeton St, Austin, Texas 78712, USA*

[2] *Department of Imaging Physics, M.D. Anderson Cancer Center, Houston, Texas 77030, USA*

* *kostia@mail.utexas.edu*

Abstract: Gold nanorods (NRs) are attractive for *in vivo* imaging due to their high optical cross-sections and tunable absorbance. However, the feasibility of using NRs for cell tracking has not been fully explored. Here, we synthesized dye doped silica-coated NRs as multimodal contrast agents for imaging of macrophages – immune cells which play an important role in cancer and cardiovascular diseases. We showed the importance of silica coating in imaging of NR-labeled cells. Photoacoustic (PA) imaging of NRs labeled macrophages showed high sensitivity. Therefore, these results provide foundation for applications of silica-coated NRs and PA imaging in tracking of immune cells.

OCIS codes: (170.0170) Medical optics and biotechnology; (170.5120) Photoacoustic imaging; (170.2655) Functional monitoring and imaging; (170.2520) Fluorescence microscopy; (060.4230) Multiplexing; (160.4236) Nanomaterials

References and links

1. P. Jha, D. Golovko, S. Bains, D. Hostetter, R. Meier, M. F. Wendland, and H. E. Daldrup-Link, "Monitoring of natural killer cell immunotherapy using noninvasive imaging modalities," Cancer Res. **70**(15), 6109–6113 (2010).
2. C. E. Green, T. Liu, V. Montel, G. Hsiao, R. D. Lester, S. Subramaniam, S. L. Gonias, and R. L. Klemke, "Chemoattractant signaling between tumor cells and macrophages regulates cancer cell migration, metastasis and neovascularization," PLoS ONE **4**(8), e6713 (2009).
3. H. Hong, Y. Yang, Y. Zhang, and W. Cai, "Non-invasive cell tracking in cancer and cancer therapy," Curr. Top. Med. Chem. **10**(12), 1237–1248 (2010).
4. I. F. Tannock, C. M. Lee, J. K. Tunggal, D. S. Cowan, and M. J. Egorin, "Limited penetration of anticancer drugs through tumor tissue: A potential cause of resistance of solid tumors to chemotherapy," Clin. Cancer Res. **8**(3), 878–884 (2002).
5. A. H. Kyle, L. A. Huxham, D. M. Yeoman, and A. I. Minchinton, "Limited tissue penetration of taxanes: A mechanism for resistance in solid tumors," Clin. Cancer Res. **13**(9), 2804–2810 (2007).
6. M. R. Choi, K. J. Stanton-Maxey, J. K. Stanley, C. S. Levin, R. Bardhan, D. Akin, S. Badve, J. Sturgis, J. P. Robinson, R. Bashir, N. J. Halas, and S. E. Clare, "A cellular Trojan Horse for delivery of therapeutic nanoparticles into tumors," Nano Lett. **7**(12), 3759–3765 (2007).
7. L. C. Kennedy, A. S. Bear, J. K. Young, N. A. Lewinski, J. Kim, A. E. Foster, and R. A. Drezek, "T cells enhance gold nanoparticle delivery to tumors in vivo," Nanoscale Res. Lett. **6**(1), 283 (2011).
8. L. M. Ricles, S. Y. Nam, K. Sokolov, S. Y. Emelianov, and L. J. Suggs, "Function of mesenchymal stem cells following loading of gold nanotracers," Int. J. Nanomedicine **6**, 407–416 (2011).
9. S. Y. Nam, L. M. Ricles, L. J. Suggs, and S. Y. Emelianov, "*In vivo* ultrasound and photoacoustic monitoring of mesenchymal stem cells labeled with gold nanotracers," PLoS ONE **7**(5), e37267 (2012).
10. A. A. Oraevsky, A. A. Karabutov, S. V. Solomatin, E. V. Savateeva, V. A. Andreev, Z. Gatalica, H. Singh, and R. D. Fleming, "Laser optoacoustic imaging of breast cancer in vivo," Proc. SPIE **4256**, 6–15 (2001).
11. X. Wang, Y. Pang, G. Ku, X. Xie, G. Stoica, and L. V. Wang, "Noninvasive laser-induced photoacoustic tomography for structural and functional in vivo imaging of the brain," Nat. Biotechnol. **21**(7), 803–806 (2003).
12. S. Mallidi, G. P. Luke, and S. Emelianov, "Photoacoustic imaging in cancer detection, diagnosis, and treatment guidance," Trends Biotechnol. **29**(5), 213–221 (2011).
13. K. Sokolov, M. Follen, J. Aaron, I. Pavlova, A. Malpica, R. Lotan, and R. Richards-Kortum, "Real-time vital optical imaging of precancer using anti-epidermal growth factor receptor antibodies conjugated to gold nanoparticles," Cancer Res. **63**(9), 1999–2004 (2003).

#195769 - $15.00 USD Received 14 Aug 2013; revised 30 Sep 2013; accepted 21 Oct 2013; published 24 Oct 2013

14. B. M. Reinhard, M. Siu, H. Agarwal, A. P. Alivisatos, and J. Liphardt, "Calibration of dynamic molecular rulers based on plasmon coupling between gold nanoparticles," Nano Lett. **5**(11), 2246–2252 (2005).
15. J. S. Aaron, N. Nitin, K. Travis, S. Kumar, T. Collier, S. Y. Park, M. José-Yacamán, L. Coghlan, M. Follen, R. Richards-Kortum, and K. V. Sokolov, "Plasmon resonance coupling of metal nanoparticles for molecular imaging of carcinogenesis in vivo," J. Biomed. Opt. **12**(3), 034007 (2007).
16. S. Mallidi, T. Larson, J. Aaron, K. Sokolov, and S. Emelianov, "Molecular specific optoacoustic imaging with plasmonic nanoparticles," Opt. Express **15**(11), 6583–6588 (2007).
17. M. C. Skala, M. J. Crow, A. Wax, and J. A. Izatt, "Photothermal optical coherence tomography of epidermal growth factor receptor in live cells using immunotargeted gold nanospheres," Nano Lett. **8**(10), 3461–3467 (2008).
18. S. Mallidi, T. Larson, J. Tam, P. P. Joshi, A. Karpiouk, K. Sokolov, and S. Emelianov, "Multiwavelength photoacoustic imaging and plasmon resonance coupling of gold nanoparticles for selective detection of cancer," Nano Lett. **9**(8), 2825–2831 (2009).
19. A. Wax and K. Sokolov, "Molecular imaging and darkfield microspectroscopy of live cells using gold plasmonic nanoparticles," Laser Photon. Rev. **3**(1-2), 146–158 (2009).
20. T. A. Larson, P. P. Joshi, and K. Sokolov, "Preventing protein adsorption and macrophage uptake of gold nanoparticles via a hydrophobic shield," ACS Nano **6**(10), 9182–9190 (2012).
21. L. R. Hirsch, R. J. Stafford, J. A. Bankson, S. R. Sershen, B. Rivera, R. E. Price, J. D. Hazle, N. J. Halas, and J. L. West, "Nanoshell-mediated near-infrared thermal therapy of tumors under magnetic resonance guidance," Proc. Natl. Acad. Sci. U.S.A. **100**(23), 13549–13554 (2003).
22. C. Loo, A. Lin, L. Hirsch, M.-H. Lee, J. Barton, N. Halas, J. West, and R. Drezek, "Nanoshell-enabled photonics-based imaging and therapy of cancer," Technol. Cancer Res. Treat. **3**(1), 33–40 (2004).
23. J. M. Stern, J. Stanfield, W. Kabbani, J.-T. Hsieh, and J. A. Cadeddu, "Selective prostate cancer thermal ablation with laser activated gold nanoshells," J. Urol. **179**(2), 748–753 (2008).
24. S. K. Baek, A. R. Makkouk, T. Krasieva, C. H. Sun, S. J. Madsen, and H. Hirschberg, "Photothermal treatment of glioma; an in vitro study of macrophage-mediated delivery of gold nanoshells," J. Neurooncol. **104**(2), 439–448 (2011).
25. J. Chen, D. Wang, J. Xi, L. Au, A. Siekkinen, A. Warsen, Z.-Y. Li, H. Zhang, Y. Xia, and X. Li, "Immuno gold nanocages with tailored optical properties for targeted photothermal destruction of cancer cells," Nano Lett. **7**(5), 1318–1322 (2007).
26. X. Yang, S. E. Skrabalak, Z. Y. Li, Y. Xia, and L. V. Wang, "Photoacoustic tomography of a rat cerebral cortex in vivo with au nanocages as an optical contrast agent," Nano Lett. **7**(12), 3798–3802 (2007).
27. K. H. Song, C. Kim, C. M. Cobley, Y. Xia, and L. V. Wang, "Near-infrared gold nanocages as a new class of tracers for photoacoustic sentinel lymph node mapping on a rat model," Nano Lett. **9**(1), 183–188 (2009).
28. Y. Xia, W. Li, C. M. Cobley, J. Chen, X. Xia, Q. Zhang, M. Yang, E. C. Cho, and P. K. Brown, "Gold nanocages: From synthesis to theranostic applications," Acc. Chem. Res. **44**(10), 914–924 (2011).
29. H. Wang, T. B. Huff, D. A. Zweifel, W. He, P. S. Low, A. Wei, and J.-X. Cheng, "In vitro and in vivo two-photon luminescence imaging of single gold nanorods," Proc. Natl. Acad. Sci. U.S.A. **102**(44), 15752–15756 (2005).
30. N. J. Durr, T. Larson, D. K. Smith, B. A. Korgel, K. Sokolov, and A. Ben-Yakar, "Two-photon luminescence imaging of cancer cells using molecularly targeted gold nanorods," Nano Lett. **7**(4), 941–945 (2007).
31. N. Chanda, R. Shukla, K. V. Katti, and R. Kannan, "Gastrin releasing protein receptor specific gold nanorods: breast and prostate tumor avid nanovectors for molecular imaging," Nano Lett. **9**(5), 1798–1805 (2009).
32. A. Wei, Q. Wei, and A. P. Leonov, "Gold nanorods as theranostic agents," in *Nanoplatform-based molecular imaging*, X. Chen, ed. (John Wiley & Sons, Inc., 2011), pp. 659–681.
33. C. L. Bayer, Y.-S. Chen, S. Kim, S. Mallidi, K. Sokolov, and S. Emelianov, "Multiplex photoacoustic molecular imaging using targeted silica-coated gold nanorods," Biomed. Opt. Express **2**(7), 1828–1835 (2011).
34. J. V. Jokerst, M. Thangaraj, P. J. Kempen, R. Sinclair, and S. S. Gambhir, "Photoacoustic imaging of mesenchymal stem cells in living mice via silica-coated gold nanorods," ACS Nano **6**(7), 5920–5930 (2012).
35. J. Choi, J. Yang, D. Bang, J. Park, J. S. Suh, Y. M. Huh, and S. Haam, "Targetable gold nanorods for epithelial cancer therapy guided by near-ir absorption imaging," Small **8**(5), 746–753 (2012).
36. P. P. Joshi, S. J. Yoon, W. G. Hardin, S. Emelianov, and K. V. Sokolov, "Conjugation of antibodies to gold nanorods through fc portion: Synthesis and molecular specific imaging," Bioconjug. Chem. **24**(6), 878–888 (2013).
37. T. P. Gustafson, Q. Cao, S. T. Wang, and M. Y. Berezin, "Design of irreversible optical nanothermometers for thermal ablations," Chem. Commun. (Camb.) **49**(7), 680–682 (2012).
38. P. K. Jain, K. S. Lee, I. H. El-Sayed, and M. A. El-Sayed, "Calculated absorption and scattering properties of gold nanoparticles of different size, shape, and composition: Applications in biological imaging and biomedicine," J. Phys. Chem. B **110**(14), 7238–7248 (2006).
39. C. Yu and J. Irudayaraj, "Multiplex biosensor using gold nanorods," Anal. Chem. **79**(2), 572–579 (2007).
40. A. Agarwal, S. W. Huang, M. O'Donnell, K. C. Day, M. Day, N. Kotov, and S. Ashkenazi, "Targeted gold nanorod contrast agent for prostate cancer detection by photoacoustic imaging," J. Appl. Phys. **102**(6), 064701 (2007).
41. H. Cui and X. Yang, "In vivo imaging and treatment of solid tumor using integrated photoacoustic imaging and high intensity focused ultrasound system," Med. Phys. **37**(9), 4777–4781 (2010).

#195769 - $15.00 USD Received 14 Aug 2013; revised 30 Sep 2013; accepted 21 Oct 2013; published 24 Oct 2013

42. A. Taruttis, E. Herzog, D. Razansky, and V. Ntziachristos, "Real-time imaging of cardiovascular dynamics and circulating gold nanorods with multispectral optoacoustic tomography," Opt. Express **18**(19), 19592–19602 (2010).
43. X. Huang, I. H. El-Sayed, W. Qian, and M. A. El-Sayed, "Cancer cell imaging and photothermal therapy in the near-infrared region by using gold nanorods," J. Am. Chem. Soc. **128**(6), 2115–2120 (2006).
44. J. Shah, S. Park, S. Aglyamov, T. Larson, L. Ma, K. Sokolov, K. Johnston, T. E. Milner, and S. Y. Emelianov, "Photoacoustic imaging and temperature measurement for photothermal cancer therapy," J. Biomed. Opt. **13**(3), 034024 (2008).
45. E. B. Dickerson, E. C. Dreaden, X. Huang, I. H. El-Sayed, H. Chu, S. Pushpanketh, J. F. McDonald, and M. A. El-Sayed, "Gold nanorod assisted near-infrared plasmonic photothermal therapy (pptt) of squamous cell carcinoma in mice," Cancer Lett. **269**(1), 57–66 (2008).
46. F. Ratto, P. Matteini, S. Centi, F. Rossi, and R. Pini, "Gold nanorods as new nanochromophores for photothermal therapies," J Biophotonics **4**(1-2), 64–73 (2011).
47. G. J. Nusz, S. M. Marinakos, A. C. Curry, A. Dahlin, F. Höök, A. Wax, and A. Chilkoti, "Label-free plasmonic detection of biomolecular binding by a single gold nanorod," Anal. Chem. **80**(4), 984–989 (2008).
48. X. Huang, S. Neretina, and M. A. El-Sayed, "Gold nanorods: From synthesis and properties to biological and biomedical applications," Adv. Mater. **21**(48), 4880–4910 (2009).
49. L. Tong, Q. Wei, A. Wei, and J.-X. Cheng, "Gold nanorods as contrast agents for biological imaging: Optical properties, surface conjugation and photothermal effects," Photochem. Photobiol. **85**(1), 21–32 (2009).
50. M. M. Arnida, M. M. Janát-Amsbury, A. Ray, C. M. Peterson, and H. Ghandehari, "Geometry and surface characteristics of gold nanoparticles influence their biodistribution and uptake by macrophages," Eur. J. Pharm. Biopharm. **77**(3), 417–423 (2011).
51. B. Nikoobakht and M. A. El-Sayed, "Preparation and growth mechanism of gold nanorods (nrs) using seed-mediated growth method," Chem. Mater. **15**(10), 1957–1962 (2003).
52. Y.-S. Chen, W. Frey, S. Kim, K. Homan, P. Kruizinga, K. Sokolov, and S. Emelianov, "Enhanced thermal stability of silica-coated gold nanorods for photoacoustic imaging and image-guided therapy," Opt. Express **18**(9), 8867–8878 (2010).
53. H. Shi, X. He, K. Wang, Y. Yuan, K. Deng, J. Chen, and W. Tan, "Rhodamine b isothiocyanate doped silica-coated fluorescent nanoparticles (rbitc-dsfnps)-based bioprobes conjugated to annexin v for apoptosis detection and imaging," Nanomedicine **3**(4), 266–272 (2007).
54. A. M. Alkilany, P. K. Nagaria, C. R. Hexel, T. J. Shaw, C. J. Murphy, and M. D. Wyatt, "Cellular uptake and cytotoxicity of gold nanorods: Molecular origin of cytotoxicity and surface effects," Small **5**(6), 701–708 (2009).
55. R. Snyderman, M. C. Pike, D. G. Fischer, and H. S. Koren, "Biologic and biochemical activities of continuous macrophage cell lines p388d1 and j774.1," J. Immunol. **119**(6), 2060–2066 (1977).
56. R. Goldman, "Induction of a high phagocytic capability in p388d1, a macrophage-like tumor cell line, by 1 α, 25-dihydroxyvitamin d3," Cancer Res. **44**(1), 11–19 (1984).
57. L. L. Chen, L. Jiang, Y. L. Wang, J. Qian, and S. He, "Multilayered polyelectrolyte-coated gold nanorods as multifunctional optical contrast agents for cancer cell imaging," J. Zhejiang Univ. Sci. B **11**(6), 417–422 (2010).
58. A. K. Oyelere, P. C. Chen, X. Huang, I. H. El-Sayed, and M. A. El-Sayed, "Peptide-conjugated gold nanorods for nuclear targeting," Bioconjug. Chem. **18**(5), 1490–1497 (2007).
59. H. Ding, K.-T. Yong, I. Roy, H. E. Pudavar, W. C. Law, E. J. Bergey, and P. N. Prasad, "Gold nanorods coated with multilayer polyelectrolyte as contrast agents for multimodal imaging," J. Phys. Chem. C **111**(34), 12552–12557 (2007).
60. C. J. Murphy, A. M. Gole, J. W. Stone, P. N. Sisco, A. M. Alkilany, E. C. Goldsmith, and S. C. Baxter, "Gold nanoparticles in biology: Beyond toxicity to cellular imaging," Acc. Chem. Res. **41**(12), 1721–1730 (2008).
61. C. Ungureanu, R. Kroes, W. Petersen, T. A. M. Groothuis, F. Ungureanu, H. Janssen, F. W. B. van Leeuwen, R. P. H. Kooyman, S. Manohar, and T. G. van Leeuwen, "Light interactions with gold nanorods and cells: Implications for photothermal nanotherapeutics," Nano Lett. **11**(5), 1887–1894 (2011).
62. Y. S. Chen, W. Frey, S. Kim, P. Kruizinga, K. Homan, and S. Emelianov, "Silica-coated gold nanorods as photoacoustic signal nanoamplifiers," Nano Lett. **11**(2), 348–354 (2011).

Introduction

The tracking of immune cells is essential to understand the regulatory role of immune cells in pathological conditions such as cancer and cardiovascular diseases [1] that can lead to development of novel therapeutic approaches [2, 3]. Moreover, using immune cells as transport vehicles for imaging and therapeutic agents can facilitate imaging and treatment of cancer cells in vasculature inaccessible areas. Indeed, one of the major barriers in cancer treatment is inaccessibility of the avascular necrotic core of a tumor by traditional drugs. Cancer cells from these hypoxic regions can survive therapy and migrate to secondary sites causing cancer metastasis [4, 5]. Immune cells can penetrate the tumor necrotic core by following chemokines released by cancer cells that can be used as a strategy to deliver a therapeutic payload [6, 7]. Optimization of these new approaches to treatment of cancer and

#195769 - $15.00 USD Received 14 Aug 2013; revised 30 Sep 2013; accepted 21 Oct 2013; published 24 Oct 2013

other diseases requires development of sensitive imaging methods for *in vivo* tracking of immune cells.

A direct approach for immune cell tracking is to load cells with contrast agents which are suitable for *in vivo* imaging modalities. Recently, we have demonstrated that loading gold nanoparticles into endosomal compartments of stem cells does not alter cellular functions including cell viability and differentiation [8]. Furthermore, we have demonstrated that stem cells labeled with gold nanoparticles can be tracked *in vivo* using combined photoacoustic (PA) and ultrasound (US) imaging with penetration depth of several centimeters [9]. In PA imaging, the tissue is irradiated with nanosecond pulses of low energy laser light. Then, through the processes of optical absorption followed by thermal expansion, broadband acoustic waves are generated within the irradiated volume. Using an ultrasound detector, these waves can be detected and spatially resolved to provide an image. Furthermore, PA imaging can be easily combined with US imaging because both imaging modalities can share the same ultrasound sensor and associated receiver electronics [10–12]. In this combination, PA signal from nanoparticle labeled immune cells can be put in context of surrounding tissue anatomy using US imaging. Therefore, combined photoacoustic and ultrasound imaging can provide complementary information.

Gold nanoparticles, including nanospheres [13–20], nanoshells [21–24], nanocages [25–28], and nanorods [29–37] are of increasing interest to biomedical engineers due to their biocompatibility, facile surface modification and high optical cross sections which can provide strong signal in imaging modalities based on optical contrast. The optical properties of gold nanoparticles can be modulated by changing their size and shape. For example, plasmon resonance of gold nanorods is easily tuned in the red to near infrared (NIR) spectral region by changing their aspect ratio [38], facilitating simultaneous imaging of multiple biomarkers [33, 39]. Strong NIR extinction cross-sections of nanorods have been used for two-photon luminescence [29, 30] and photoacoustic [12,40–42] imaging of thick biological samples as well as for photothermal destruction of cancer cells [43–46]. Thus, anisotropic gold nanorods provide a convenient combination of properties for biomedical applications including the possibility of cell tracking using PA imaging [47–49]. However, the optical absorbance spectra of gold nanorods broaden when they interact with live cells [36]. This effect is due to plasmon resonance coupling of closely spaced nanoparticles upon cellular uptake and it diminishes the ability to simultaneously image multiple cell populations labeled with different nanorods. In addition, recent reports showed that cells more readily uptake spherical nanoparticles as compared to rod-shaped particles [50]. As spherical nanoparticles do not have the desired near infrared absorption necessary for *in vivo* imaging, increasing cellular uptake of nanorods is desirable.

Here we synthesized silica-coated gold nanorods to address the challenges associated with applications of rod-shaped gold nanoparticles in cell tracking. The silica coating changes the shape of nanorods from cylindrical to spheroidal. We demonstrated that the silica-shell reduces plasmon resonance coupling between nanorods upon uptake by cells and, thus, can facilitate multiplex imaging using nanorods. In addition, the silica shell was doped with fluorescent dye to enable multimodal imaging with fluorescence and PA imaging modalities. This combination enables in-depth *in vivo* imaging of labeled cells using photoacoustics followed by a high-resolution *ex vivo* fluorescence imaging for validation and detailed characterization of *in vivo* imaging data.

Experimental methods

Synthesis of PEG-coated gold nanorods (mPEG-NRs): Gold nanorods (NRs) were synthesized by seed mediated growth mechanism using the previously published protocol [51]. The as-prepared nanorods were washed twice in water by centrifugation at 18000g for 45 minutes. The final NRs pellet was dispersed in water and stored at room temperature at an optical density (OD) of 15. Before silica-coating, the cetyl trimethyl ammonium bromide

#195769 - $15.00 USD Received 14 Aug 2013; revised 30 Sep 2013; accepted 21 Oct 2013; published 24 Oct 2013

(CTAB) layers on NRs were replaced with methoxy-PEG-thiol (mPEG-SH). One milliliter of 1 mg/mL mPEG-SH (5kDa) in water was mixed with 1 mL of CTAB-NRs (OD 15) and sonicated using a water bath sonicator (Branson 1510R-MT) for 1 minute at room temperature. After sonication, the NRs were stirred overnight in presence of mPEG-SH to complete the replacement of CTAB. Free CTAB and mPEG-SH molecules were removed by centrifugation through 100kDa centrifugal filters at 2500g for 15 minutes. Then, the NRs were washed one more time in water to remove any residual mPEG and CTAB. mPEG-NRs were dispersed in 1 mL water and stored at room temperature.

Synthesis of silica-coated gold nanorods: Fluorescent silica-coated gold nanorods were synthesized by covalent attachment of a fluorescent dye (Rhodamine) to the silica matrix (Fig. 1). Silica shells of controlled thickness were deposited on the PEG-coated nanorods using a modified Stöber method [52]. One milliliter of mPEG-NRs (OD 15) was mixed with 1.5 mL of isopropanol. The solution was continuously stirred while adding 0.6 mL of 3 vol % tetraethylorthosilicate (TEOS) and 0.625 mL of 3.84 vol % ammonium hydroxide (NH_4OH). Rhodamine (Rh) dye doped silica-coated nanorods (RhSilicaNRs) were synthesized by first covalently attaching Rh isothiocyanate dye to [3-(2-Aminoethylamino)propyl]trimethoxysilane (AEAPTMS) [53]. Briefly, 15 µL of [3-(2-Aminoethylamino)propyl]trimethoxysilane was stirred with 10 mg Rhodamine B isothiocyanate in 2.5 mL of anhydrous isopropanol (IPA) for 48 hours under nitrogen. This solution was five times diluted in anhydrous IPA just prior to using. One milliliter of mPEG-NRs (OD 15) was mixed with 1.5 mL of isopropanol. The solution was continuously stirred while adding 0.6 mL of 3 vol % tetraethylorthosilicate (TEOS) and 0.625 mL of 3.84 vol % ammonium hydroxide (NH_4OH). After 30 minutes, four aliquots (12.5 µL each) of the diluted Rhodamine-AEAPTMS solution were added to the reaction mixture (TEOS:Rh-AEAPTMS molar ratio 1080:1). The aliquots were separated by 10 minutes time intervals. After 2 hours of stirring at room temperature, the silica-coated nanorods were collected by centrifugation at 700g for 15 minutes using 100 kDa MWCO centrifugal filters. Both plain SilicaNRs and RhSilicaNRs were washed three times with water prior to use.

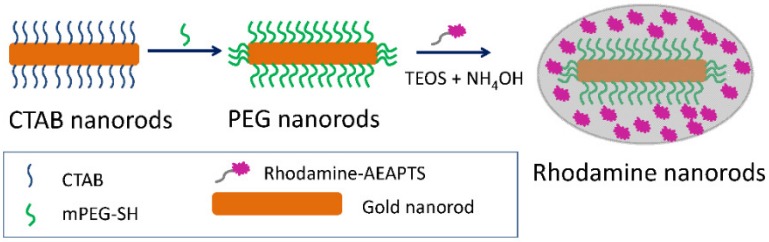

Fig. 1. Schematic of approach used to synthesize fluorescent silica-coated nanorods.

Synthesis of polymer-coated nanorods: Polymer-coated nanorods were synthesized by mixing 1 mL of CTAB-coated gold nanorods (OD 10) with 1 mL of polystyrene sulfonate (PSS) solution (10 mg PSS per 1 mL of 1 mM NaCl) [30, 54]. The solution was kept on a shaker for 30 minutes and then centrifuged at 18000g for 15 minutes. The nanorods containing pellet was redispersed in 1 mL of 1 mM NaCl solution and was mixed with 1 mL of PSS solution. The solution was placed on a shaker for 30 minutes and then centrifuged to collect the nanorods coated with PSS. The PSS-nanorods were coated with Poly(allylamine hydrochloride) (PAH) using the same procedure. PSS-nanorods pellet was dispersed in a 1 mL NaCl solution (1 mM) and mixed with 1 mL of PAH solution (10 mg PAH per mL of 1 mM NaCl). After 30 minutes of shaking, the nanorods pellet was collected using centrifugation and dispersed in a salt solution. The PAH coating procedure was repeated once more to obtain PAH-PSS-nanorods. The final nanorods pellet was dispersed in 1 mM NaCl solution.

#195769 - $15.00 USD Received 14 Aug 2013; revised 30 Sep 2013; accepted 21 Oct 2013; published 24 Oct 2013

Cell viability study: The viability of monocyte/macrophage (RAW 264.7) cells was performed after incubating the cells with RhSilicaNRs at a given concentration in phenol-free DMEM cell culture media for 18 hours at 37°C. As the nanorods-loaded cells need to be viable for a long period of time for successful tracking of cells, extended cell viability tests were performed by culturing cells in regular cell culture media for an additional 24 to 48 hours after the incubation of cells with silica-nanorods. To perform cell viability study, cells were washed once with PBS and a background absorbance was measured at 490 nm using BioTek Synergy HT UV-Vis spectrophotometer. Then MTS reagent (mixture of MTS and PMS prepared in cell culture media) was added to the cells. After 3 hours of incubation with MTS solution, absorbance at 490 nm was measured again and the background absorbance values were subtracted in order to determine the number of metabolically active live cells in a sample.

Two mouse-macrophage cell lines, RAW 264.7 and P388D1, were used for cell labeling and characterization throughout this study. While RAW 264.7 cells are highly phagocytic macrophage cells, P388D1 cells have an inferior phagocytic activity [55, 56]. In order to achieve camparable loading of nanorods in both cell lines, we used higher dosage of $1x10^7$ NRs/cell for P388D1 cells as compared to $7x10^4$ NRs/cell for RAW 264.7. The cells were incubated with nanorods for 18 hours at 37°C in cell culture media. Labeled cells were washed with cell culture media to remove any unbound nanorods and re-suspended in phenol free media to measure absorbance. Absorbance spectra of unlabeled cells were subtracted from the spectra of nanorod-loaded cells to obtain the contribution from nanorods. Before the measurements, cells were counted using a standard hemocytometer in the presence of trypan blue; trypan blue is a vital stain that selectively colors dead and lysed cells. More than 95% of cells were vital during the absorption measurements.

Tissue mimicking phantom preparation: Gelatin based tissue-mimicking phantoms with cell inclusions were fabricated for combined photoacoustic and ultrasound imaging. To simulate tissue background, 8wt% gelatin solution with 0.2wt% of 15 μm silica particles was used to prepare the base and top layers which encapsulated the cell inclusions. Suspensions of P388D1 cells only and P388D1 cells loaded with RhSilicaNRs were mixed with the same volume of 16wt% gelatin solution at 37°C. Specifically, five inclusions of P388D1 cells loaded with RhSilicaNRs were prepared with cells concentrations 5×10^6, 2.5×10^6, 1.25×10^6, 2.5×10^5, and 1.25×10^5 cells/mL. For the cells only inclusion, 5×10^6 cells/mL cell concentration was used. For phantom preparation, suspension of silica particles in gelatin at 37°C was poured in a petri dish and was cooled down at 4°C. During the cool down step, some silica particles settle down that results in a reduced ultrasound contrast in the top part of the phantom. Then, suspensions of cells in gelatin were placed on the solidified base layer and were allowed cool down. Finally, the top layer of gelatin/silica particles was added to complete the phantom.

Photoacoustic imaging set-up: The photoacoustic signal from the tissue-mimicking phatom was obtained using a Vevo® 2100 LAZR imaging system (VisualSonics, Inc., Toronto, Canada) and an array ultrasound transducer (LZ250, VisualSonics, Inc.) operating at 20 MHz center frequency. A laser beam with 5 ns pulses and 20 Hz repetition rate was generated by a tunable OPO laser system pumped by Nd:YAG laser. The wavelength of the light in this experiment was matched to the peak optical absorption wavelength of the silica-nanorods, which is 780 nm. The laser beam was delivered through an optical fiber bundle integrated with the ultrasound array transducer. A mechanical system was used to translate the transducer to allow for collecting multiple cross-sectional US/PA images of the inclusions in steps of 114 μm. In order to perform a quantitative photoacoustic signal comparision between each inclusion, the fluence of the laser was maintained at 10 mJ/cm^2, which is below the damage threshold for silica-nanorods [52]. To compensate amplitude of PA signal for laser fluctuations, laser fluence was recorded by the VEVO 2100 LAZR imaging system during PA imaging and PA signals were normalized by corresponding laser fluences in post-

#195769 - $15.00 USD Received 14 Aug 2013; revised 30 Sep 2013; accepted 21 Oct 2013; published 24 Oct 2013

processing. PA signal intensity of each inclusion was measured by averaging PA signals from 11 different cross-sectional images of the inclusion.

Results and discussion

The RhSilicaNRs were characterized using TEM and fluorescence emission. Transmission electron microscopy showed a uniform silica layer on the coated nanorods (Fig. 2(a)). The fluorescence emission spectrum of the RhSilicaNRs indicated successful encapsulation of fluorescent dye in the silica-coated nanorods (Fig. 2(b)).

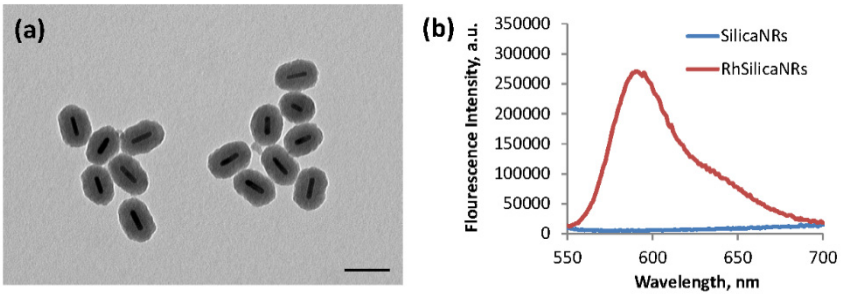

Fig. 2. (a) Transmission Electron Microscopy of Rhodamine silica-coated nanorods (RhSilicaNRs), scale bar: 100 nm; (b) fluorescence emission spectra of RhSilicaNRs (ex 540 nm) and plain silica-coated nanorods (SilicaNRs).

Cellular tracking requires long term viability of nanoparticle-loaded cells. Here we used a monocyte macrophage cell line (RAW 264.7) to evaluate extended viability of cells loaded with flourescent silica-coated and PEG-coated nanorods following 18 hours of incubation. The nanorod-loaded macrophages were grown in cell culture media for 24 and 48 hours before testing cell viability using MTS assay that measures metabolic activity of live cell and also reflects the number of viable cells. Most of macrophages loaded with RhSilicaNRs showed no change or a slight increase in metabolic activity possibly due to macrophage activation by the nanoparticle uptake. A slight decrease in viability of cells loaded with mPEG-NRs after 24 hours culture can be attributed to a small amount of residual CTAB molecules which are present after ligand exchange with PEG [36].

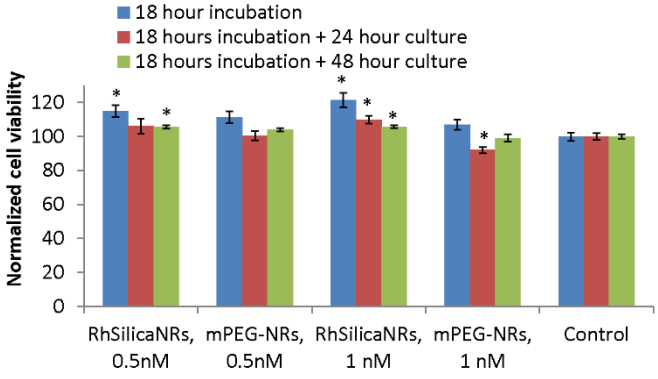

Fig. 3. Viability of mouse monocyte macrophage cell line (RAW 264.7) loaded with mPEG-NRs and RhSilicaNRs immediately after 18 hrs of incubation with nanoparticles and 24 and 48 hours of cell culture after the incubation. RhSilicaNRs show no toxicity during extended cell culture of labeled cells. Statistically different results based on student t-test (p-value < 0.01) are identified by (*).

Silica-coated nanorods exhibit negligible changes in the longitudinal peak position and the full-width at half-maximum (FWHM) values after uptake by two macrophage cells lines -

#195769 - $15.00 USD Received 14 Aug 2013; revised 30 Sep 2013; accepted 21 Oct 2013; published 24 Oct 2013

RAW 264.7 and P388D1 (Fig. 4(a), 4(b) and Table 1). In contrast, nanorods coated using layer-by-layer deposition of polystyrene sulfonate (PSS) and poly(allylamine hydrochloride) (PAH) polymers [57] show significant change in the optical absorption upon cellular uptake (Fig. 4(c), Table 1). Note that RhSilicaNRs, SilicaNRs and PAH-PSS-NRs have different longitudinal peak maxima. These results demonstrate that silica coating of *ca.* 30 nm provides sufficient spacing to prevent plasmon resonance coupling of nanorods after they are uptaken by live cells. Since silica-coated gold nanorods do not change optical spectra inside cells, we used extinction coefficients of the nanorods in suspension to determine nanorod loading of cells. RAW 264.7 and P388D1 cells accumulated *ca.* 10^4 and $2x10^4$ silica-coated nanorods per cell, respectively. Cells loaded with RhSilicaNRs can be readily viasualized using fluorescence imaging (Fig. 5(e) and 5(f)). Negligible nanorod-specific contrast was observed in the dark-field images of RhSilicaNRs-loaded cells due to low sensitivity of our optical microscope to NIR logitudinal resonances of the nanorods used in this study (Fig. 5(b) and 5(c)). Thus, fluorescence imaging provides a convenient way of identifying cells labeled with dye-dopped silica-coated gold nanorods.

Previous literature reports have shown a good contrast in dark-field imaging of gold nanorods with a longitudinal peak in the visible range [58, 59]. It has been also reported by us [36] and other groups [43, 60, 61] that cells loaded or labeled with gold nanorods coated by a thin layer of organic ligands and targeting biomolecules produce detectable contrast in dark-field images as compared to unlabeled cells. We attribute this contrast to aggregation of gold nanorods upon cellular uptake that results in an overall increase in scattering in the visible region due to plasmon resonance coupling between closely spaced nanoparticles. In the present study, silica coating around nanorods significantly diminishes the effect of plasmon resonance coupling as described above and, therefore, silica-coated nanorods do not provide significant contrast in the presence of endogenous scattering background from cells.

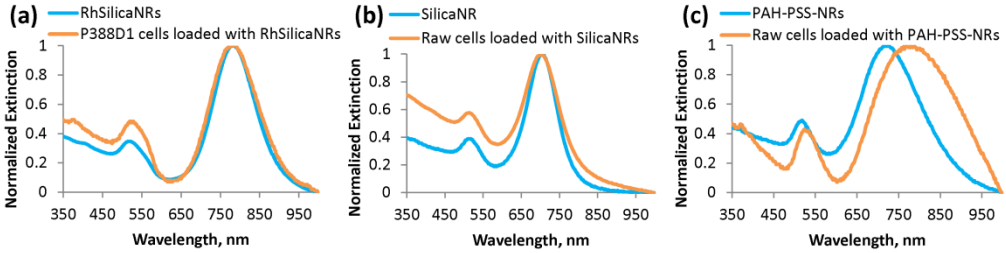

Fig. 4. Extinction spectra of: (a) RhSilicaNRs in suspension and P388D1 cells loaded with RhSilicaNRs; (b) SilicaNRs in suspension and RAW 264.7 cells loaded with SilicaNRs; (c) polymer-coated nanorods (PAH-PSS-NRs) in suspension and RAW 264.7 cells loaded with PAH-PSS-NRs. Longitudinal peak position and extinction spectra of silica-coated nanorods do not undergo significant changes after cell uptake in contrast to polymer-coated NRs.

Table 1. Characterization of absorbance spectra of nanorods and cells-loaded with nanorods; FMHM – full width at half maximum.

	FWHM, nm	% Increase in FWHM	Longitudinal Peak Wavelength, nm
RhSilicaNRs	120		782
P388D1 cells with RhSilicaNRs	138	15.00%	778
SilicaNRs	83		704
RAW 264.7 cells with SilicaNRs	87	4.82%	700
PAH-PSS-NRs	139		725
RAW 264.7 cells with PAH-PSS-NRs	222	59.71%	800

#195769 - $15.00 USD Received 14 Aug 2013; revised 30 Sep 2013; accepted 21 Oct 2013; published 24 Oct 2013

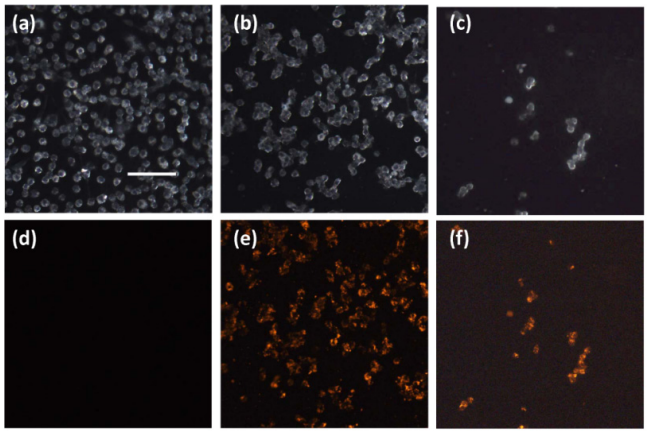

Fig. 5. Dark-field (a, b, c) and fluorescence (d, e, f) images of RAW 264.7 cells alone (a, d), RAW 264.7 cells loaded with RhSilicaNRs (b, e) and P388D1 cells loaded with RhSilicaNRs (c, f). Scale bar 50 μm. Images were acquired with Leica DM600 upright microscope using 20x 0.5 NA objective. Fluorescence imaging was performed using Cy3 filter cube, ex/em 555/590 nm.

Having successfully loaded cells with silica-coated nanorods, the next step was to evaluate the feasibility of sensitive detection of the nanorod-loaded cells using PA imaging. To this end, inclusions containing different concentrations of P388D1 cells loaded with RhSilicaNRs were incorporated in the tissue-mimicking phantoms and multiple cross-sectional PA images of each inclusion were collected at 780 nm wavelength, which corresponds to the longitudinal plasmon resonance peak of the nanorods (Fig. 6). Although the same matrix was used to prepare the top and bottom layers of the phantom, settlement of silica particles in the bottom layer of the phantom results in a decreased US contrast at the boundary between the top and the bottom layers (approximately in the middle of the images on Fig. 6(a). The PA signal intensity showed linear behavior as a function of concentration of labeled cells (the R^2 value for the linear regression fit is 0.9753). From the linear regression fit in Fig. 6(b), we determined that PA imaging can detect *ca.* 1.25 x 10^6 cells evenly dispersed in a 1 cm^3 volume. After taking into account the imaging kernel size of the photoacoustic system of approximately 160 μm x 110 μm x 220 μm, we calculated that PA imaging could detect as few as five nanorod-loaded cells per imaging kernel.

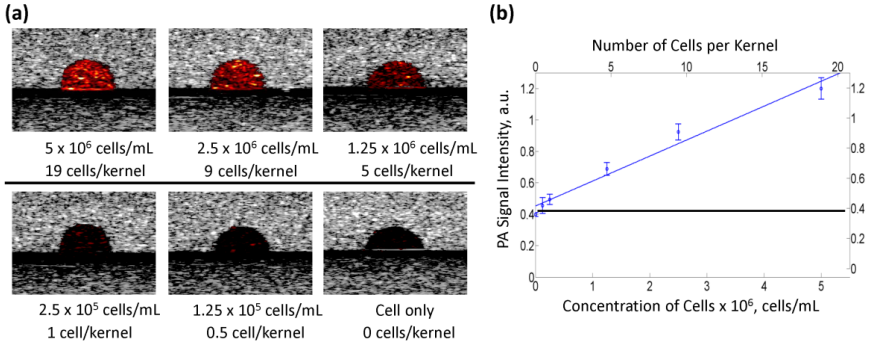

Fig. 6. Photoacoustic images of tissue-mimicking phantoms prepared with different concentrations of P388D1 cells loaded with Rh-Silica-NRs (a). Each image covers a 6.3 x 8.8 mm field of view. Dependence of PA signal amplitudes on concentration of nanorod-loaded cells at 780 nm excitation wavelength (b); the top horizontal axis shows a number of cells per imaging kernel size of the photoacoustic system of approximately 160 μm x 110 μm x 220 μm. The solid blue line represents the linear regression fit of the data and the black line shows the noise level in PA imaging (b).

#195769 - $15.00 USD Received 14 Aug 2013; revised 30 Sep 2013; accepted 21 Oct 2013; published 24 Oct 2013

Conclusions

In summary, we systematically addressed challenges associated with applications of gold nanorods in cell imaging. First, we demonstrated long-term biocompatibility of fluorescent silica-coated nanorods for cell tracking experiments. Then, we showed that silica-coated nanorods do not alter optical properties upon cellular uptake that can facilitate multiplex imaging of various cell populations. Furthermore, our previous studies demonstrated that silica coating increases stability [52] and signal strength [62] of gold nanorods in PA imaging. The combination of these properties that are afforded by silica coating results in the detection limit of just few labeled cells in tissue mimicking phantoms. These promising results provide the foundation for applications of silica-coated gold nanorods and PA imaging in tracking of immune cells in studies ranging from the mechanistic understanding of immune responses in cancer and cardiovascular diseases to the cell mediated delivery of therapy.

Acknowledgments

This research was supported by National Institute of Health grants EB008101, HL096981 and CA149740. We also would like to thank Ms. Maria Jimenez for proofreading the manuscript.

#195769 - $15.00 USD Received 14 Aug 2013; revised 30 Sep 2013; accepted 21 Oct 2013; published 24 Oct 2013